Julia Walther, Christian Schnabel, Florian Tetschke, Tobias Rosenauer, Jonas Golde, Nadja Ebert, Michael Baumann, Christian Hannig, Edmund Koch

In vivo imaging in the oral cavity by endoscopic optical coherence tomography

Erstveröffentlichung in / First published in:

Journal of Biomedical Optics. 2018 (23), S. 071207-1 – 071207-13 [Zugriff am: 02.05.2019]. SPIE Digital Library. ISSN 1560-2281.

DOI: https://doi.org/10.1117/1.JBO.23.7.071207

Journal of Biomedical Optics

BiomedicalOptics.SPIEDigitalLibrary.org

In vivo imaging in the oral cavity by endoscopic optical coherence tomography

Julia Walther
Christian Schnabel
Florian Tetschke
Tobias Rosenauer
Jonas Golde
Nadja Ebert
Michael Baumann
Christian Hannig
Edmund Koch

Julia Walther, Christian Schnabel, Florian Tetschke, Tobias Rosenauer, Jonas Golde, Nadja Ebert, Michael Baumann, Christian Hannig, Edmund Koch, "*In vivo* imaging in the oral cavity by endoscopic optical coherence tomography," *J. Biomed. Opt.* **23**(7), 071207 (2018), doi: 10.1117/1.JBO.23.7.071207.

Journal of Biomedical Optics 23(7), 071207 (July 2018)

In vivo imaging in the oral cavity by endoscopic optical coherence tomography

Julia Walther,[a,b,*] Christian Schnabel,[a] Florian Tetschke,[c] Tobias Rosenauer,[c] Jonas Golde,[a] Nadja Ebert,[d,e] Michael Baumann,[d,e,f,g] Christian Hannig,[c] and Edmund Koch[a]

[a]TU Dresden, Faculty of Medicine Carl Gustav Carus, Anesthesiology and Intensive Care Medicine, Clinical Sensoring and Monitoring, Dresden, Germany
[b]TU Dresden, Faculty of Medicine Carl Gustav Carus, Department of Medical Physics and Biomedical Engineering, Dresden, Germany
[c]TU Dresden, Faculty of Medicine Carl Gustav Carus, Policlinic of Operative and Pediatric Dentistry, Dresden, Germany
[d]TU Dresden, Faculty of Medicine Carl Gustav Carus, Department of Radiotherapy and Radiooncology, Dresden, Germany
[e]TU Dresden, Faculty of Medicine Carl Gustav Carus, OncoRay–National Center of Radiation Research in Oncology, Dresden, Germany
[f]Helmholtz-Zentrum Dresden-Rossendorf, Institute of Radiooncology, Dresden, Germany
[g]German Cancer Research Center (DKFZ) and German Cancer Consortium (DKTK), Heidelberg, Germany

Abstract. The common way to diagnose hard and soft tissue irregularities in the oral cavity is initially the visual inspection by an experienced dentist followed by further medical examinations, such as radiological imaging and/or histopathological investigation. For the diagnosis of oral hard and soft tissues, the detection of early transformations is mostly hampered by poor visual access, low specificity of the diagnosis techniques, and/or limited feasibility of frequent screenings. Therefore, optical noninvasive diagnosis of oral tissue is promising to improve the accuracy of oral screening. Considering this demand, a rigid handheld endoscopic scanner was developed for optical coherence tomography (OCT). The novelty is the usage of a commercially near-infrared endoscope with fitting optics in combination with an established spectral-domain OCT system of our workgroup. By reaching a high spatial resolution, *in vivo* images of anterior and especially posterior dental and mucosal tissues were obtained from the oral cavity of two volunteers. The convincing image quality of the endoscopic OCT device is particularly obvious for the imaging of different regions of the human soft palate with highly scattering fibrous layer and capillary network within the lamina propria. [DOI: 10.1117/1.JBO.23.7.071207]

Keywords: optical coherence tomography; endoscopic imaging; dentistry; medical and biological imaging optics; medical optics instrumentation; tissue.

Paper 170533SSPRR received Aug. 10, 2017; accepted for publication Jan. 11, 2018; published online Mar. 2, 2018.

1 Introduction

Visual examination is usually the first step toward diagnosis of diseases within the oral cavity, such as carious lesions, periodontitis, oral inflammation, dysplasia, and malignancies. Sometimes, the recognition and diagnosis of altered tissue, even by an experienced physician or dentist may be difficult and imprecise, especially in early stages of pathologic phenomena. Due to the multiplicity of diseases of the oral cavity, commonly coupled with changes in tissue structure, high resolution diagnostic imaging modalities in routine clinical dentistry and maxillofacial surgery are beneficial for the detection and treatment of lesions. Current imaging modalities in dentistry include conventional x-ray radiography, computed and digital volume tomography (CT, DVT), magnetic resonance tomography (MRI), and sonography (ultrasound, US) for the *in vivo* diagnosis of altered tissue in the oral cavity. While all of those imaging techniques are well established, the diagnosis of submillimeter structure is still difficult (for e.g., US) or rather expensive in clinical routine (e.g., CT/DVT, MRI). Present reliable diagnosis of pathological changes in soft tissues, such as the oral mucosa, gingiva, and tongue, normally requires repeated biopsy and histological examination of conspicuous lesions with the drawback of delayed detection of malignant changes for curative treatment. In addition, versatile appearance of mucosal tissue alterations, in combination with absent routine inspection of patients for oral lesions, may lead to late diagnosis. Therefore, effective diagnostic modalities would be of exceptional clinical relevance. Latest established optical imaging methods for *in vivo* detection of mucosal changes are spectroscopy and confocal imaging, which are still challenging in clinical routine due to small field-of-views (FoV) and low penetration depths. A complementary imaging technique is optical coherence tomography (OCT) providing cross sections (B-scans) and volume views of tissue microstructures of depths up to 1 to 2 mm with the feature of detecting changes in tissue scattering.[1–4] Even though OCT does not deliver subcellular resolution or molecular contrast, it has the potential of label-free optical biopsies of tissue *in vivo* by a simple noninvasive subsurface view to assess depth structures of oral soft and hard tissue lesions. Most research has presented the feasibility of OCT in various preclinical animal[5–7] and human[8–10] oral cavity studies. Although OCT enables functional imaging, such as Doppler OCT,[11–13] polarization-sensitive OCT[14–16] and spectroscopic OCT,[17,18] the core strength of oral examination by OCT convincingly lies in the easily applied morphological imaging valued by a physician similar to US examinations.

*Address all correspondence to Julia Walther, E-mail: julia.walther@tu-dresden.de

In dental research, as a main field of application with regard to the oral cavity, OCT has become a promising approach for the investigation of the dental microstructure. So far, the majority of studies using OCT in dentistry are based on *ex vivo* investigations, either with artificial alteration models or at inactive lesions on extracted teeth. Nevertheless, a small number of promising dental OCT studies dealing with the *in vivo* detection of caries lesions can be found.[19–23] Compared to the current gold standard of radiographic examination, OCT provides a higher spatial resolution and contrast for hard tissue and allows the discrimination of enamel and dentin, as well as the recognition of the dentin–enamel junction (EDJ).[24,25] Furthermore, de- and remineralization processes can be measured[26,27] and thus makes OCT suitable for the spatially resolved detection of early pathologic changes.[28–31] Moreover, OCT overcomes the drawbacks of superimposed imaging with ionizing radiation and enables the observation of short-term progression in carious dental hard tissue.[32,33] Since the decision for or against invasive treatment is dependent on the progress of a lesion, this information could be of great value for the clinician.[34] On the other hand, the application of OCT is limited by the relatively low penetration depth, compared to the radiographic imaging.

In oral cancer diagnosis, as another application field regarding the oral cavity, the structural imaging by OCT for early and/or differentiating detection of malign tissue has to be assessed critically. OCT provides assessment of the entire epithelium and partly the underlying lamina propria (LP) and has the potential to distinguish normal from pathologic mucosal tissue of different entities.[5,6,35–39] The distinction between normal and pathologic tissue is mainly based on the measurement of the epithelial thickness, the identification of the adjacent basement membrane, and the vasculature within the LP, as well as the changed backscattering behavior of the altered tissue lesions. The most promising approach in this context is the potential for biopsy guidance by OCT in conjunction with an improvement of diagnostic accuracy of biopsies.[40–42]

Since OCT is a promising imaging modality for the noninvasive *in vivo* examination of oral soft and hard tissue, the demand for intraoral miniaturized or rather endoscopic OCT (EOCT) optics is substantial especially for the accessibility of the posterior oral cavity.[43] Although a variety of impressive EOCT solutions are proposed in flexible catheter-based configuration,[44,45] especially for intravascular,[46] bronchial[47] as well as gastrointestinal diagnosis,[48,49] in rigid implementation, in particular, for otorhinolaryngology[50–52] and in needle-like design for intratissue examinations in cancer diagnosis,[53–56] developments of intraoral OCT probes adapted to the oral cavity can only be found occasionally.[57–59] So far, rigid handheld endoscopic probes,[20,60–63] miniaturized probes,[64,65] and rotary pullback catheters[66,67] are developed in forward and side viewing configuration, as well as in contact and noncontact mode for intraoral measurements, which is a crucial step for the application of OCT methodology in clinical practice. In our judgment, most of the reported rigid OCT systems allow the imaging of the well accessible buccal mucosa, the hard and anterior soft palate as well as different parts of the tongue, but none of them has demonstrated contactless OCT images of different areas of the posterior oral mucosa (e.g., palatoglossal arch and fold) with highly resolved structures of the connective tissue and molars *in vivo*.

The aim of the present study is to expand intraoral application of OCT by a simple adaption of a commercially available endoscope. The development of a handheld endoscopic forward viewing OCT probe enables high quality two- and three-dimensional imaging of teeth and mucosa of the anterior and posterior oral cavity to pave the way for *in vivo* noninvasive tissue biopsy. The potential of the presented imaging system is demonstrated by *in vivo* measurements of healthy oral mucosa and conspicuous parts of teeth by means of two volunteers.

2 Endoscopic System Setup

2.1 *Specification of the Rigid Endoscopic Optics*

In this research, the rigid endoscopic optics used for OCT imaging of the oral cavity is a commercially available near-infrared (NIR) endoscope from Karl Storz GmbH & Co. KG. The NIR endoscope has an insertion diameter of 10 mm, a length of 200 mm, and an angle of view of 0 deg (instrument axis consistent with optical axis) and is assumed to be based on afocal optics with a 0.25-fold magnification. For a center wavelength of $\lambda_{\text{center}} = 580$ nm, a lateral resolution of $\Delta x = 62.5$ μm at a working distance of WD ~49 mm is determined by means of an externally illuminated USAF resolution test target (USAF-1951-target) in combination with a proximally positioned VIS camera focused to infinity. In order to get a focus on the distal side of the endoscope and to increase the lateral resolution, the optics in front of the proximal end of the endoscope was simply adapted. As a result, a lateral resolution of $\Delta x = 12.4$ μm at WD ~7.5 mm and $\lambda_{\text{center}} = 580$ nm is achieved [cf. Fig. 1(b)], which corresponds to $\Delta x = 17.9$ μm for the NIR wavelength range with $\lambda_{\text{center}} = 835$ nm under the assumption of $\Delta x \sim \lambda_{\text{center}}$. The FoV in dependency on WD is determined by a millimeter paper test chart with the result of a linear relationship with a slope of $m = 1.1$, as shown in Fig. 2(c).

2.2 *Endoscopic Optical Coherence Tomography System Setup*

The OCT system used in this study is spectrometer-based and consists of a fiber-coupled superluminescent diode (SLD-371-HP1, Superlumdiodes Ltd., Ireland) with a central wavelength of 835 nm and a FWHM of 50 nm, an optical circulator (CIR-0850-40-APC, Thorlabs GmbH, Germany), a fiber-coupled Michelson interferometer and a self-developed spectrometer with a wavelength range from 802 to 867 nm. As presented in Fig. 3, the scanning EOCT probe is equipped with a collimator C1 (Schäfter + Kirchhoff GmbH, Germany), two galvanometer scanners GS_x and GS_y (Cambridge Technology Inc., USA) for 2-D beam deflection, a lens combination consisting of two achromats L1+L2 for light coupling (Edmund Optics GmbH,

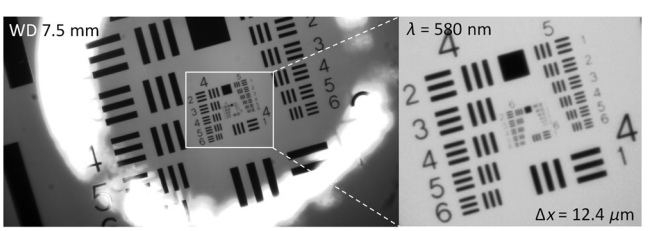

Fig. 1 By adapting the proximal optics for light coupling, a lateral resolution of $\Delta x = 12.4$ μm of the commercial NIR endoscope from Karl Storz GmbH & Co. KG is measured by means of a proximal VIS camera in combination with the USAF resolution test target, which is positioned at a working distance of WD ~7.5 mm and illuminated by a center wavelength of $\lambda_{\text{center}} = 580$ nm.

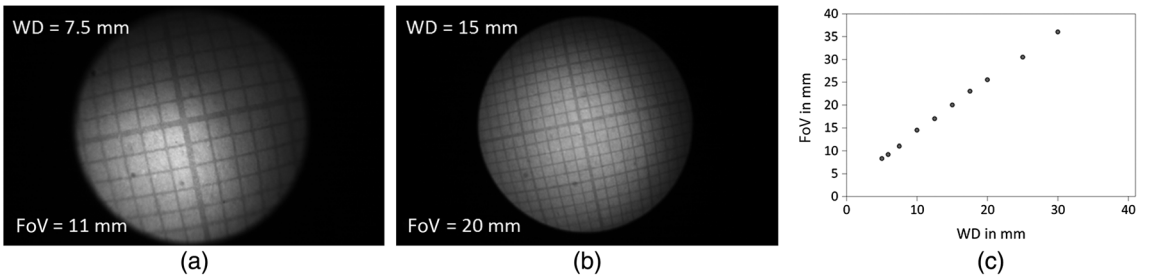

Fig. 2 (a,b) Endoscopic VIS images of a millimeter paper test chart, which is illuminated by the integrated illumination system of the endoscope, for measuring the relation between the FoV and the WD. (c) At the favorable WD of 5 to 10 mm, the FoV with fan-shaped beam increased linearly from 8.3 to 14.5 mm.

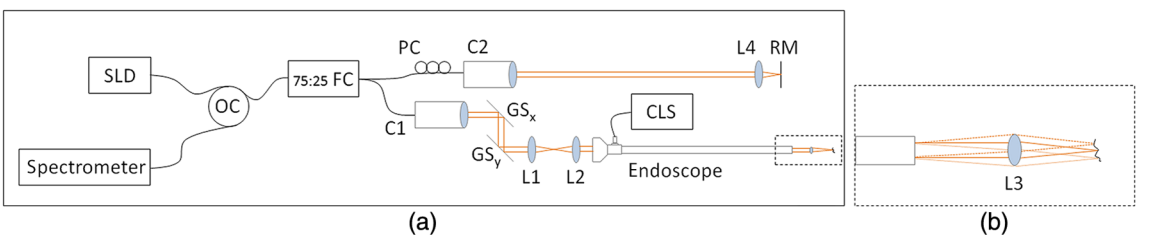

Fig. 3 (a) Scheme of the principle OCT setup. SLD, 5-mW superluminescent diode with $\lambda_{center} = 835$ nm and FWHM = 50 nm; OC, optical circulator; FC, wideband fiber coupler with a coupling ratio of 75:25; C1 and C2, collimators; GS, galvanometer scanners; L1–L4, lenses; endoscope, endoscope from Karl Storz GmbH and Co. KG; CLS, cold-light source; PC, polarization controller; RM, reference mirror; spectrometer, line rate of 11.88 kHz. (b) Telecentric imaging is realized by an additional lens L3 mounted on the distal end of the commercial endoscope at 4 mm distance by a custom adapter made of stainless steel.

Germany), the NIR endoscope from Karl Storz GmbH & Co. KG, and an additional objective lens L3 (AC050-008-B, Thorlabs GmbH, Germany; at 4-mm distance to the distal end of the endoscope) for telecentric OCT imaging. As seen, the difference in glass content between sample and reference arm is not compensated optically but numerically in the processing.[68,69]

The optical components C1, GS$_x$, GS$_y$, L1 and L2 are integrated in a base body made of polylactide (PLA), at which the chosen endoscope, a CCD VIS camera, and an ergonomic handle are mounted, as shown in Fig. 4(a). Lens L3 is pasted into an additional adapter made of stainless steel by two set screws (M2) and secured by optical glue (Vitralit®1655, Panacol-Elosol GmbH, Germany). Since the distal lens allows imaging only in a small range, a CCD camera (acA1600-20uc, Basler AG) is installed at the base body of the handheld scanner head for online off-axis video guidance by means of an overview image of the oral cavity [cf. Fig. 4(a), yellow beam path], which is displayed on the integrated LCD screen (LCDInfo Oy, Finland). The custom-developed spectrometer, operating at a read-out rate of 11.88 kHz for one A-scan, is mounted in an OCT table device [cf. Fig. 4(b)] along with the SLD and the optical circulator, as well as the drive electronics of the galvanometer scanners and electronic control of the line scan detector (Dalsa IL C6, Teledyne DALSA Inc., Canada).[70] The control of the system, the data acquisition, and online display are

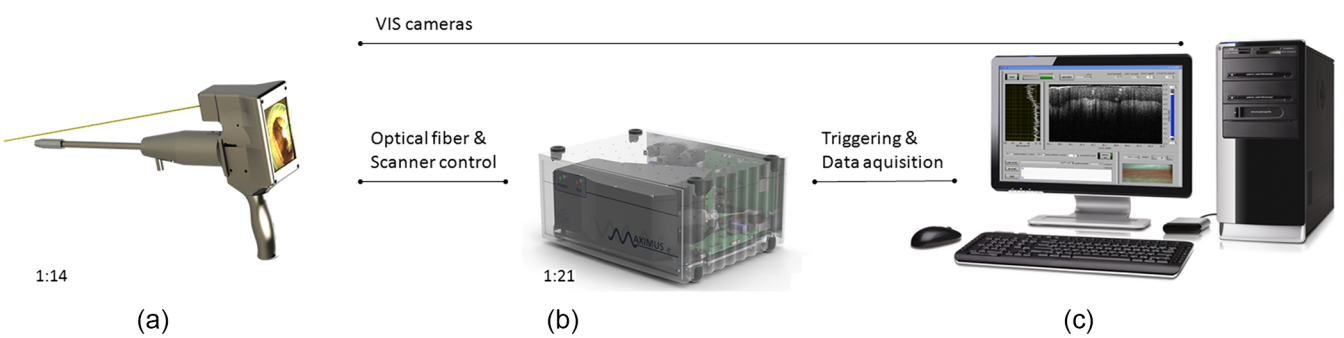

Fig. 4 Scheme of the measurement setup for the endoscopic investigation of the oral cavity equipped with (a) the EOCT probe with integrated scanning sample arm, (b) the base OCT device with built-in SLD, spectrometer, partial fiber optics and system electronics, and (c) a personal computer for the control and triggering of the electronic components as well as the data display and acquisition.

controlled by custom software developed with LabVIEW® (National Instruments Inc., USA) on a personal computer [cf. Fig. 4(c)]. With typical 480 A-scans per frame (B-scan), the system achieves ~23 frames/s, which can be processed and displayed in real time.

The overall dimensions of the developed scanner head including the proximal handle are 76 mm × 442 mm × 251 mm (width × depth × height) with an endoscopic part relevant for the mouth of a length of 200 mm and a diameter of 15 mm tapered to 10 mm at the distal end [cf. Fig. 15 in Appendix]. The height of the scanner body is mainly defined by the height of the handle (100 mm) and the height of the LCD screen (130 mm). With this design, most of the oral cavity is reached proven by two experienced dentists and one physician. Limitation of the developed endoscope might occur for the imaging of the buccal side and the interdental space of second and third molars of patients with reduced mouth opening. The endoscopic probe enables imaging in noncontact and contact mode by using an additional spacer (distance piece), which is simply mounted on the lens adapter of lens L3 before medical examination and acts as a disposable item for future clinical use. Advantageously, the endoscope, considered as an attachment to the scanner head, can be cleaned and disinfected (by immersing into 3% Sekusept® aktiv solution, Ecolab Deutschland GmbH, Germany) in the daily hospital routine. If necessary, steam sterilization can be performed by disconnecting the commercial endoscope.

2.3 *EOCT Scanner Performance*

In order to evaluate the performance of the developed EOCT probe with telecentric scanning, several measurements were performed for the quantification of the axial and lateral resolution $(\Delta z, \Delta x)$, the FoV, the sensitivity, and the spectrometer-induced depth-dependent sensitivity loss. The axial resolution of the OCT system without the endoscopic extension is experimentally measured to be $\Delta z = 11$ μm in air and in good agreement with the theoretical value of $\Delta z = 10.8$ μm. The measurement range is 2.75 mm. Since the glass content in the sample arm is higher than in the reference arm, the occurring dispersion mismatch is numerically compensated for optimal resolution.[68,71] This is achieved by multiplying the spectral data (which is formerly linearized in k-space, zero-padded to 2^{12} pixels and spectrally shaped) with a compensating phase term $e^{-i\varphi(k)}$.[69,72] The empirically determined phase correction amounts to

$$\varphi(k) = a\left(\frac{k-k_0}{\Delta k}\right)^2 + b\left(\frac{k-k_0}{\Delta k}\right)^3 \quad \text{with} \quad a = 150 \text{ rad} \quad \text{and} \quad b = 3 \text{ rad}, \tag{1}$$

where the coefficient a is the dominant second order term, compensating the group velocity dispersion, and with this, the broadening of the axial resolution in OCT, and coefficient b is the very low third-order term eliminating the asymmetric distortion. k_0 is the mean wavenumber and Δk is the half width of the spectrum captured with the detector, so that the terms within the brackets of Eq. (1) run from −1 to +1. The comparison of the experimentally obtained quadratic term of the compensating phase shift with data calculated from the Schott glass database results in glass length from 75 mm of SF66 up to 620 mm of NFK51A or any appropriate mixture of glasses. As the total length of the endoscope is 265 mm in addition to lenses in the base body of the scanner, this result seems to be reasonable. However, this calculation does not allow a more accurate insight into the glass composition of the endoscope. The cubic term of the phase shift gives no additional information on the glass type as this is ~2% of the quadratic term for most glasses considering the spectral range of this OCT system. The experimentally obtained axial resolution of $\Delta z = 11.6$ μm in air ($\Delta z = 8.7$ μm in tissue) is measured by means of the reflection of a glass plate and corresponds approximately to the one achieved with the scanner head without endoscope.[73] The lateral resolution is measured by telecentric OCT imaging of the USAF resolution test target and amounts to $\Delta x = 17.5$ μm [cf. Fig. 5(a)], which confirms the measurement result in Sec. 2.1. The FoV, achieved with the telecentric OCT imaging (cf. Fig. 3), is determined by means of the mm-paper target and results in $x_{max} = y_{max} = 4.8$ mm, as depicted in Fig. 5(b).

The sensitivity is obtained from a glass substrate surface (−14 dB reflector) and amounts to −88 dB. Due to the decreasing resolvability of interference signals with increasing frequency on the line detector of the spectrometer, a signal loss of 8 dB (sensitivity-roll-off) between zero and maximum depth is determined.

3 Endoscopic Optical Coherence Tomography Imaging in the Oral Cavity

3.1 *Dental Imaging*

The most promising application fields for OCT in dentistry are (1) the detection of carious lesions and the characterization of

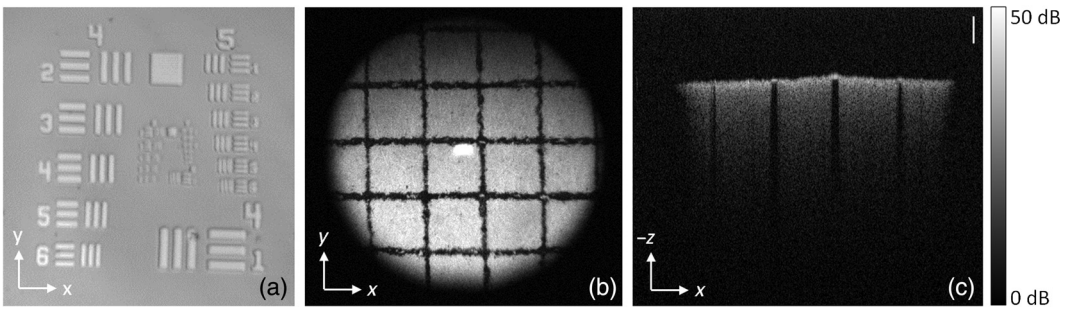

Fig. 5 *En face* projection of the USAF-1951-target (a) as well as a millimeter-chart (b) detected by telecentric EOCT for determining the lateral resolution and the FoV. (c) Corresponding OCT cross-sectional image (B-scan) of the millimeter-chart endoscopically detected. Scale bar in the cross-sectional image (c) corresponds to 500 μm in air.

(de)mineralization processes, (2) the detection of defects at dental restorations, and (3) the assessment of erosion and cracks. Particularly for the imaging of well-defined boundaries, such as the interfacial layer between a dental restoration and the natural tooth surface, OCT might be a beneficial tool for the dentist to assess internal defects.[74,75]

For testing the developed EOCT system at dental hard tissue, two volunteers were examined (A: male 30 years, B: female 33 years). Prior to the OCT measurements, oral examination was made by an experienced dentist in order to select specific regions for imaging. Additionally, photographic overviews of the oral cavity were made for the allocation of the imaged regions. First, OCT measurements of the incisors of volunteer A are performed with the handheld scanner head in noncontact mode. In order to reduce movement artifacts for the imaging of the premolars and molars, the distal end of the endoscope is equipped with an attached distance piece, which is positioned at the region of interest of the tooth.

Figure 6 shows the photograph of the maxillary central incisors [Figs. 6(a) and 6(b)] as well as the OCT B-scans [Figs. 6(c)–6(e)] at the corresponding lines in the zoom view in Fig. 6(b). In Fig. 6(c), the proximal region of tooth 11 and tooth 21 was imaged [at the red line in Fig. 6(b)]. The EDJ can be recognized by a well-defined, low-scattering band between the enamel (E) and the dentin (D).[19,24,25] Conspicuously, the enamel of both tooth 11 and 21 appears as light-dark progression containing homogeneous bands of varying intensity, which is assumed to be caused by the birefringent properties. In former research, it was shown that enamel appears as layered structure in polarization-sensitive (PS) OCT.[76,77] Although the light source is not polarized, the system presented in this work is sensitive to birefringence.[78] Figure 6(d) shows a shadow artifact caused by a strong scattering microcrack in the upper region of the enamel [asterisk, cf. Refs. 31, 79, and 80, at the green line in Fig. 6(b)]. Due to increased scattering, higher intensities and a reduced penetration depth of the OCT signal can be observed at the gingiva in Fig. 6(e) [cf. Refs. 57, 75, and 81, at the blue line in Fig. 6(b)].

The composite restoration (CR) at tooth 11 [cf. magenta frame in Fig. 6(b)] is characterized by a homogeneous scattering layer in the OCT B-scans, as presented in Figs. 7(a) and 7(b). Interfacial gaps (green arrow in a) or even small cracks (green arrow in b) are visible at different positions in the restoration, which was found by previous nonendoscopic *ex vivo* research results.[31,74,82,83] The 3-D representation reveals a roughened intersectional profile of the restoration (c,d). There, two projections were chosen: (c) with manually manipulated sectional view (artificial edges marked in bright green) to image the interfacial gap of the composite restoration in the three-dimensional context and (d) with intact and untreated surface of the imaged composite-enamel-passage.

Beyond the OCT imaging at the maxillary central incisors, the first premolars of both volunteers were examined by the developed EOCT scanner head. The upper row in Fig. 8 [parts 8(a)–8(c)] represents the OCT B-scan and 3-D projection of the cervical area of tooth 24 in subject B, showing the exposed dentin at the transition to the gingiva. Furthermore, a small white spot can be identified in the reduced enamel layer without clear diagnosis. The OCT examination of the mineralization defect at tooth 24 in subject A can be recognized by a high scattering band in the OCT scan in Figs. 8(d) and 8(e), appearing in a depth up to 430 μm. Again, the normal enamel (E) appears as light-dark changes in the right image part in Fig. 8(d).

EOCT measurements were performed up to the region of the posterior teeth. A small fracture at the buccal side of tooth 16 in subject A is shown in Fig. 9. The B-scan and 3-D representation indicate that also the subjacent enamel layer is affected by the fracture. As already shown at the microcrack in Fig. 6(d), a shadowing effect due to higher backscattering of the incident light at the breakage can be found below the inset fractures.

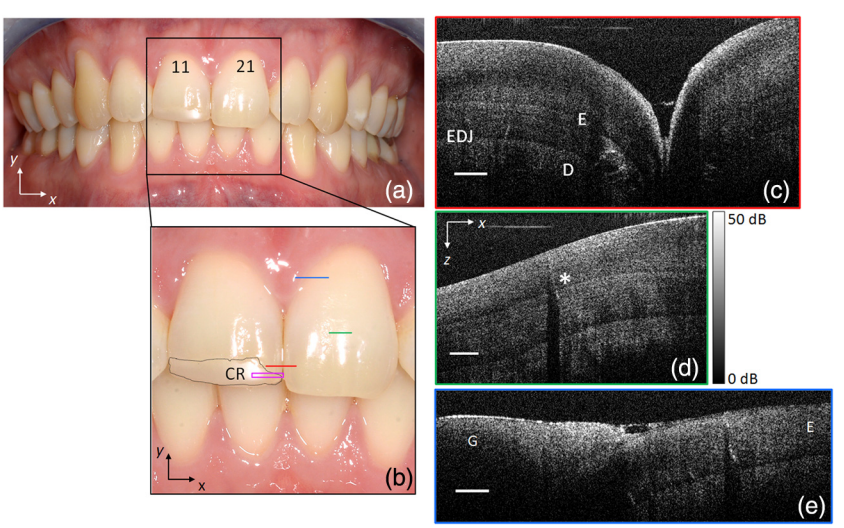

Fig. 6 (a) Photographic overview and (b) magnification of the maxillary central incisors with corresponding exemplary OCT B-scans of the proximal region between tooth 11 and 21 (c, red), the enamel (E), the EDJ and the dentin (D) of tooth 11 (d, green) with breakage (asterisk), and the intersection between enamel and gingiva (e, blue). The OCT measurement was performed in noncontact mode. Abbreviations: E, enamel; D, dentin; EDJ, enamel–dentin junction; G, gingiva; CR, composite restoration. Coordinate system in (d) is equivalent in image part (c) and (e). Scale bar in the OCT images (c–e) corresponds to 300 μm. Indicated dynamic range is valid for all depicted OCT images.

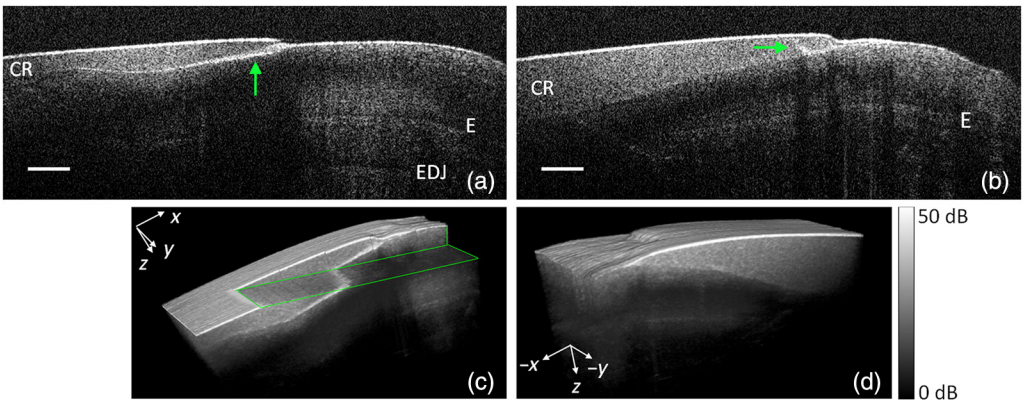

Fig. 7 Cross-sectional images (a, b) and 3-D representation (c, d) of the composite restoration (CR) within the magenta frame in Fig. 6(b). Green arrows show gaps (a) or even small cracks (b) in the restoration. The dental surface of the 3-D display in panel (c) is manually manipulated in the postprocessing (artificial edges marked in bright green) to provide a more instructive view of the interfacial gap of the composite restoration. Again, the OCT measurement was performed in noncontact mode. Abbreviations: E, enamel; EDJ, enamel–dentin junction; CR, composite restoration. Scale bar in (a) and (b) corresponds to 300 μm. Indicated dynamic range is valid for all depicted OCT images.

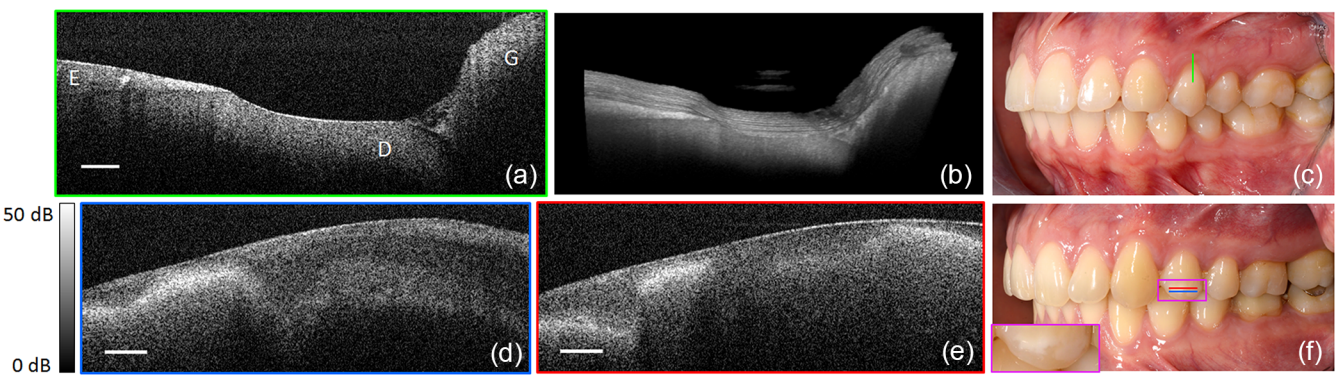

Fig. 8 Upper row shows a single exemplary OCT B-scan (a) and generated 3-D scan (b) of the cervical area of tooth 24 of subject B (c). The OCT examination was performed contactless. Lower row presents the OCT results of the mineralization defect at tooth 24 of proband A (f) in 2-D (d,e). The second *in vivo* OCT measurement (d,e) was realized in contact mode by an additional distance piece (disposable item) at the distal endoscopic end. Abbreviations: E, enamel; D, dentin; G, gingiva. Scale bar in part (a), (d), and (e) corresponds to 300 μm. Indicated dynamic range is valid for all depicted OCT images.

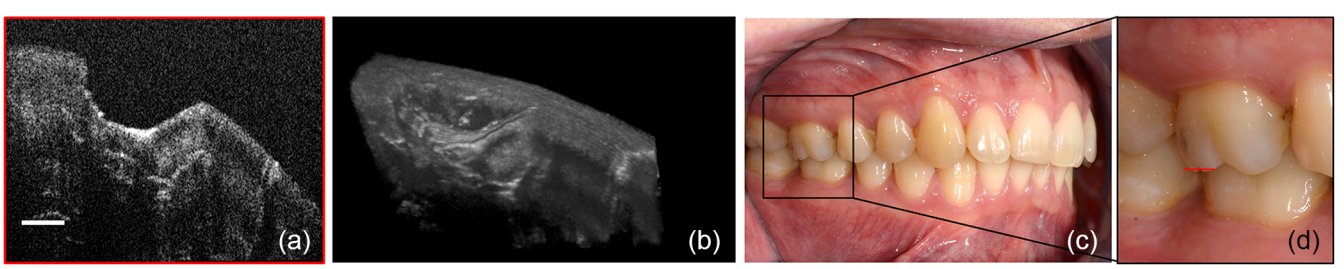

Fig. 9 Exemplary B-scan (a) and 3-D representation (b) of a fracture at the buccal area of tooth 16 in subject A. The *in vivo* OCT imaging was executed in contact mode by the aid of a distal distance piece (disposable item). Scale bar in (a) corresponds to 300 μm. Dynamic range of the depicted OCT cross-sectional scans amounts to 50 dB.

In addition, occlusal surfaces, such as the mesial-occlusal-distal composite restoration at tooth 45, in subject A, were imaged as exemplary presented in Fig. 10. The intersection between the restoration and the surrounding enamel shows a smooth transition without major cracks or gaps. The appearing bright section inside the restoration [cf. Fig. 10(b)] could be caused by an interlayer, possibly resulting from air entrapments or from varying scattering properties of adhesive and composite.

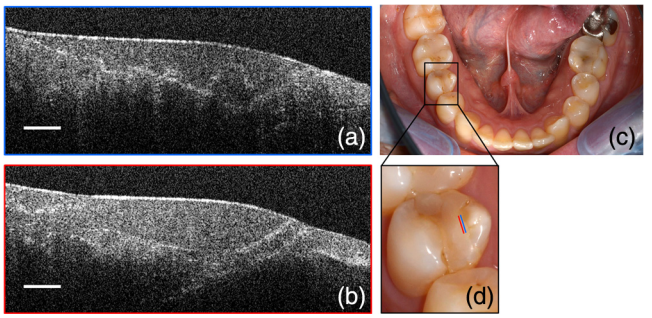

Fig. 10 (a,b) Representative B-scans of a mesial–distal–occlusal composite restoration at (c,d) tooth 45 in subject A. The *in vivo* OCT measurement was realized in contact mode by an additional distal distance piece (disposable item). Scale bar in (a) and (b) corresponds to 300 μm. Dynamic range of the depicted OCT cross-sectional scans amounts to 50 dB.

3.2 *Imaging of the Oral Mucosa*

For characterizing the performance of the handheld EOCT probe at the oral soft tissue, the mucosa at different parts of the oral cavity is imaged by means of a healthy volunteer (subject B in Sec. 3.1: female, 33 years, nonsmoker, occasional use of alcohol). Of particular interest for OCT imaging is the lining mucosa, which enables a larger depth of light penetration due to the absence of a corneous layer in comparison to the masticatory mucosa, such as the gingiva [cf. Fig. 6(e)], which is covered by keratinized stratified squamous epithelium. Figure 11 displays three exemplary B-scans of the buccal mucosa of subject B. With regard to the structural validation of oral mucosal tissue in OCT images by Hamdoon et al.,[38] the epithelial layer (EP) has a lower backscattering signal and appears more homogenous in comparison to the subsequent LP, which is confirmed by the imaging results in Fig. 11. The lower signal intensity of normal epithelium is related to the lower optical density and scattering properties.[9] The LP corresponds to a dense fibrous layer with embedded blood vessels and nerves, which can be clearly differentiated from EP due to the higher backscattering signal and inhomogeneity in the OCT cross-sections. The EP and LP are divided by a basement membrane, which appears as a demarcation line between the two different backscattering signals of EP and underlying LP. OCT scans were acquired at the anterior [cf. Figs. 11(a) and 11(b)] and the posterior [cf. Fig. 11(c)] buccal mucosa. The epithelial thickness of the buccal mucosa is measured to be maximum 500 μm in the anterior part and of about 300 μm in the posterior region of the inside of the cheek.

Additionally, the oral mucosa of the tongue and lateral floor of the mouth is imaged contactless by EOCT. Figure 12

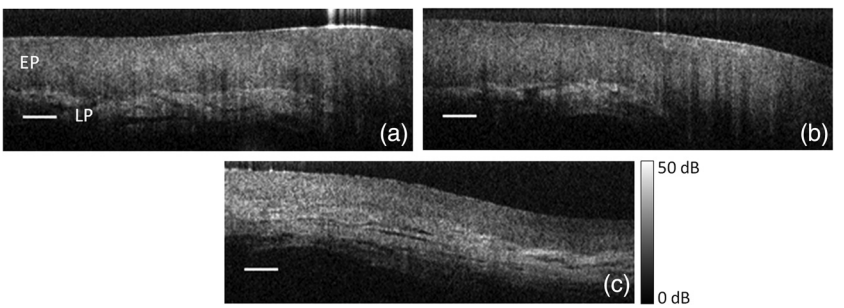

Fig. 11 Single exemplary B-scans of the buccal oral mucosa *in vivo*, which are detected contactless at selected regions of the inner surface of the human cheek. (a, b) Buccal oral mucosa toward the human mouth in the anterior region of the oral cavity. (c) Buccal oral mucosa toward the oropharynx in the posterior region of the oral cavity. The OCT measurement was performed in noncontact mode. Abbreviations: EP, epithelium; LP, lamina propria. Scale bar: 300 μm. Indicated dynamic range is valid for all depicted OCT images.

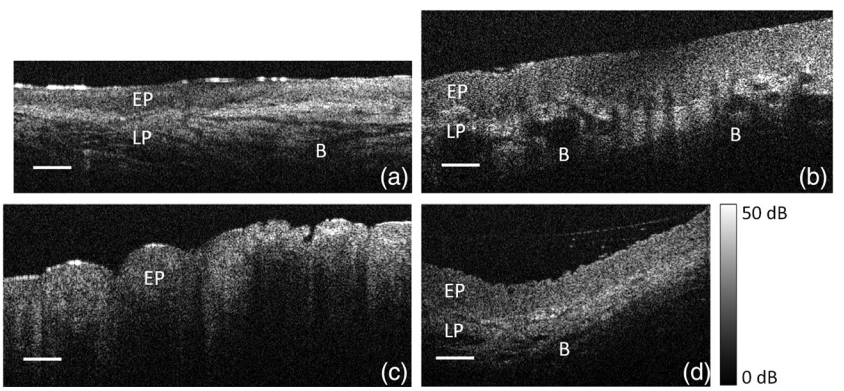

Fig. 12 Single exemplary B-scans showing (a) the oral mucosa *in vivo* of the inferior surface of the human tongue (facies inferior linguae), (b) the margin of the tongue (margo linguae), (c) the dorsum of the tongue (dorsum linguae), and (d) the lateral floor of the mouth. All measurements are carried out in noncontact mode. Abbreviations: EP, epithelium; LP, lamina propria; B, blood vessel. Scale bar: 300 μm. Indicated dynamic range is valid for all depicted OCT images.

demonstrates OCT cross-sectional images of the tongue body especially the inferior surface (a), the lateral border (b), and the curved upper surface (dorsum) (c). As a result, the EP thickness of the tongue strongly depends on its location and lowest for the inferior surface of the tongue with its smooth mucous membrane and thin stratified squamous epithelium [cf. Fig. 12(a)]. Additionally, the sublingual vessel network and the dense fibrous layer within the highly scattering LP are clearly visible in (a). The oral mucosa of the lateral border of the tongue in (b) shows a thicker EP, which is clearly differentiated from the subjacent LP with imaged minor and major blood vessels. In Fig. 12(c), the specialized oral mucosa of the surface of the tongue shows prominent epithelium ridges and tongue papillae. Due to the thick keratinized stratified squamous epithelium of the dorsal surface, the imaging depth is limited for which reason the LP is not visible in the OCT image [Fig. 12(c)]. An additional example for the lining mucosa is shown in Fig. 12(d), where the EP and the LP of the floor of the mouth are demonstrated.

Besides the representative OCT measurements of the buccal and lingual mucosa, the oral mucosa of the soft palate was imaged exemplarily with the developed OCT endoscope. For test purposes, the soft palate and the palatoglossal arch are examined in contact mode. In Fig. 13, the palatal mucosa is imaged by EOCT for three different regions of the soft palate. Figure 13(a) presents the oral mucosa of the anterior soft palate (toward the posterior border of hard palate), which obviously contains an LP with highly scattering dense connective tissue. This may be interpreted as part of the thin firm fibrous lamella named palatine aponeurosis. Below the dense fibrous layer, submucosal structures with integrated blood vessels are visible. In comparison, the oral mucosa detected at the palatoglossal arch is presented in Fig. 13(b) and shows a comparable EP, a thinner highly scattering fibrous layer as well as submucosal structures beneath. The oral mucosa of the transition part from the palatoglossal fold to the posterior buccal mucosa shows a varying EP thickness with a clearly determinable LP [cf. Figs. 13(c), 13(c1), and 13(c2)].

In addition, the oral mucosa of the palatoglossal arch was imaged via contactless EOCT. The results are presented in Fig. 14, where the EP and subsequent LP are obviously differentiable.

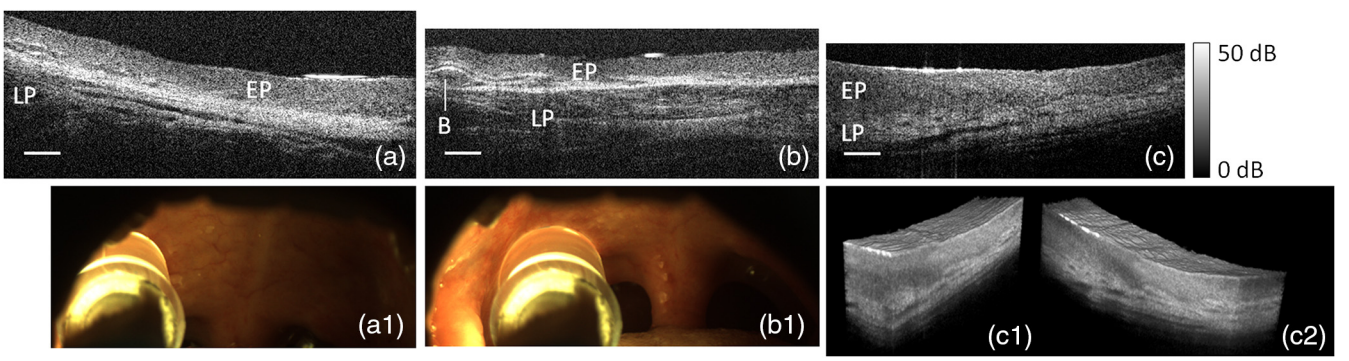

Fig. 13 (a–c) Cross-sectional images of oral mucosa at three selected regions of the soft palate, which are detected in contact mode. Oral mucosa of the anterior soft palate close to the posterior border of the hard palate (a) and corresponding overview image of the off-axis camera (a1). Oral mucosa of the central soft palate (b) and corresponding video guidance image (b1). Oral mucosa of the palatoglossal arch close to the posterior buccal mucosa in 2-D (c) and 3-D (c1,c2). Abbreviations: EP, epithelium; LP, lamina propria; B, blood vessel. Scale bar: 300 μm. Indicated dynamic range is valid for all depicted OCT images.

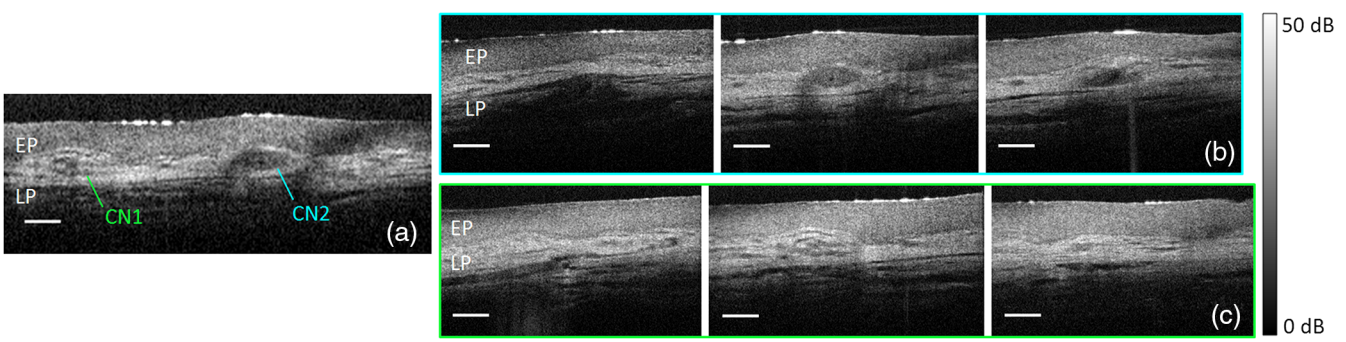

Fig. 14 Contactless OCT detection of oral mucosa of the palatoglossal arch of the soft palate with two capillary branches. (a) 2-D OCT with both capillary branches (CN1, CN2) embedded in the papillary layer of the LP. (b,c) OCT image series of the two capillary branches showing cross-section in front, through, and after the small capillary network. Abbreviations: EP, epithelium; LP, lamina propria; CN, capillary network. Scale bar: 300 μm. Indicated dynamic range is valid for all depicted OCT images.

Moreover, two capillary branches (CN1 and CN2) lying relatively close to each other are detected within the papillary layer of the LP. Both capillary branches running to the papilla are detected separately in 3-D. Representative B-scans of the OCT volume scans are presented as image series in Figs. 14(b) and 14(c), showing the respective cross-section in front, through, and after the capillary networks CN1 and CN2 within the superficial layer of the LP.

4 Discussion and Summary

In this research, customized EOCT imaging of the anterior and posterior oral cavity was allowed by adapting a commercially available NIR endoscope by Karl Storz GmbH & Co. KG. By developing a scanning optics for 2-D imaging and using the established SD-OCT system of our workgroup, EOCT cross-sections of hard and soft oral tissue are detected with a frame rate of 23 fps, a spatial resolution of 11.6 μm axially and 17.5 μm laterally, and a FoV of 4.8 mm. This allows an image quality highly appropriate for the oral optical biopsy with μm-resolution. All presented imaging results are primary generated in noncontact mode (no contact to the imaged oral tissue but possible contact of the endoscope shaft to, e.g., lips), which is preferential for the investigation of highly sensitive and painful mucous oral regions. The movements of the test person are reduced by a variable forehead and chin support similar to the eye refractometry. Despite the handheld measurement, motion artifacts have rarely been observed. Moreover, investigations are also possible in contact mode by an additional spacer (disposable item) positioned at the tissue to be investigated, which is advantageous for recording dental volumetric data with minimal motion artifacts. In general, the technical development of a handheld endoscopic probe forms the basis for *in vivo* OCT studies of physicians and dentists in the dental clinic. By this adaption, the potential support of OCT to current diagnostic tools of visual inspection and radiology, which unfortunately show insufficient sensitivity and specificity in clinical routine, can be validated.

Promising application of EOCT in the oral cavity is generally the early detection of initial and small pathologic alterations of hard and soft tissue. Considering dentistry, OCT could particularly improve the detection of early incipient demineralization and primary/secondary caries, the diagnosis of periodontal disease, the monitoring and assessment of dental restorations as well as the visualization of different dental and orthodontic treatment steps in general, which is confirmed by the presented preliminary *in vivo* endoscopic results. For caries diagnostics, the primary aim is the detection of emerging demineralization. Since these lesions are characterized by porous areas in comparison to the surrounding enamel, OCT has the potential to image these lesions as white spots positioned close to the tooth subsurface up to 2 mm in depth within the enamel. By applying the developed EOCT probe, the detection of noncavitated occlusal carious lesions of premolars and molars *in vivo* is enabled to a limited extent with regard to the interdental and labial surfaces. Considering dental restorations, the assessment of the composite homogeneity and bonding, especially at the tooth-restoration interface and margin, as well as the early detection of secondary carious lesions, is demanding. Here again, the proposed OCT endoscope enables the subsurface imaging with the exception of interdental treatments. Besides these noninvasive applications, the feasibility of supporting minimally invasive restorative treatment with a customized EOCT scanner will be evaluated in a clinical study in future research.

Regarding the oral examinations, current research is strongly focused on depth-resolved imaging of early malign tissue. OCT in general and as endoscopic adaption in particular enables the imaging of the epithelial thickness end ridges of the oral mucosa, as well as irregular epithelial stratification. Moreover, the measurement of the continuity of the basement membrane is allowed. To the best of our knowledge, OCT imaging of different regions of the human soft palate (e.g., the palatoglossal arch and fold) with highly resolved structures of the LP *in vivo* is realized for the first time by means of the presented endoscopic development. By this, the findings of previous *ex vivo* and *in vivo* studies can be expanded to the posterior oral cavity under *in vivo* conditions. By knowing the regular structure of the oral mucosa of different parts of the oral cavity accessible by the developed OCT endoscope, the differentiation of normal and morphologically altered oral tissue should be ensured prospectively.[35] Since the image quality of the presented EOCT probe offers appropriate axial and lateral resolution, even small structural alteration could be apparent, which has to be validated in a future clinical study. Despite the conspicuousness, premalignant disorders will be challenging to differentiate from benign lesions and to stage by OCT. In our view, the developed EOCT probe will have its most potential primarily in the monitoring of dysplastic lesions and further in biopsy guidance during surgical removal of lesions.

In summary, the developed EOCT probe, based on the commercially available NIR endoscope, ranks among the few *in vivo* scanners designed for the oral cavity (cf. Table 1 in Appendix) with the advantage of an expanded application field: the posterior oral cavity including different regions of the palatoglossal arch and (pre-)molars. As a result of this presented preliminary research, the contactless imaging is preferable for the examination of the soft tissue due to the high sensitivity, whereas the contact and noncontact mode is equally feasible for the hard tissue diagnosis. Besides the good image quality with high lateral and axial resolution, and sufficient wide FoV, the development convinces primarily with the accessibility to most of the oral sections and further with flexibility, efficiency, and effectiveness in the prospective clinical routine. In this research, the feasibility of *in vivo* studies within the anterior and posterior oral cavity was validly presented by hard and soft tissue imaging. The evaluation of the promising medical applications in clinical routine will be part of subsequent studies. For the case of successful studies with high reliability, accuracy, and evidence, OCT could have the potential to promote the clinical decision process in the future research.

Appendix

For the objective evaluation of the presented development, important technical specifications of previously published endoscopic probes designed for *in vivo* imaging of the human oral cavity are listed in Table 1. Moreover, a technical drawing of the handheld endoscopic scanner head is given in Fig. 15.

Disclosures

The PS-OCT imaging of the human oral cavity by the homebuilt system was reviewed and approved by the developers employed at the Technische Universität Dresden, and informed consent was obtained from all subjects before imaging. Both human

Table 1 Technical specifications of published rigid oral probes (Appendix).

Ref.	Oral regions	Spatial resolution	FoV	Technique	Contact/ Noncontact mode	Scan rate
Walther (this work)	Dental hard and soft tissue of the anterior and posterior oral cavity; in detail: buccal and lingual oral mucosa, mouth floor, palatoglossal arch and fold (soft palate), incisors, premolars and molars	Lateral 17.5 μm Axial 11 μm	4.8 mm	Rigid (commercial endoscope with Hopkins optics), handheld	Both	11.88 kHz 23 fps
Lenton et al.[20]	Tooth occlusal	Lateral 80 μm Axial 11 μm	No specs	Rigid, handheld	Contactless	30 kHz
Davoudi et al.[59]	Buccal, labial, and lingual oral mucosa, soft palate (no layered structure and no connective tissue visible)	Lateral 20.5 μm Axial 7 μm	2 mm	Rigid (no Hopkins optics), mounted on a stage	Contactless	47 kHz
Tsai et al.[60]	Buccal, labial, and lingual oral mucosa (possibly not long enough for the posterior oral cavity)	Lateral 10 μm Axial 8 μm	2 mm	Rigid (no Hopkins optics), handheld	Contact	100 kHz
Higgins and Pierce[62]	No specifications	Lateral 12.4 μm Axial 9.3 μm	2 mm	Rigid (no Hopkins optics), handheld	Contact	25.3 fps
Wang et al.[63]	Buccal, labial, and lingual oral mucosa, mouth floor, hard palate, anterior soft palate (no layered structure and no connective tissue visible)	Lateral and axial 12 μm	4.6 mm	Rigid (GRIN lens), side viewing probe, sharp edges of the endoscopic tip, handheld	Contact	13 kHz 25 fps
Wang et al.[64]	Buccal mucosa, leukoplakia tissue	Lateral 40 μm Axial 10.6 μm	2 mm	Rigid (GRIN lens), handheld	No specs	50 kHz
Sun et al.[65]	Tooth buccal	Axial 10 μm	2 to 4 mm	Rigid (fiber-based), handheld	No specs	20 kHz
Lee et al.[66]	Buccal and lingual oral mucosa	Lateral 20 to 40 μm	2.3 mm	Rigid (fiber-based), handheld	Contact	50.4 kHz

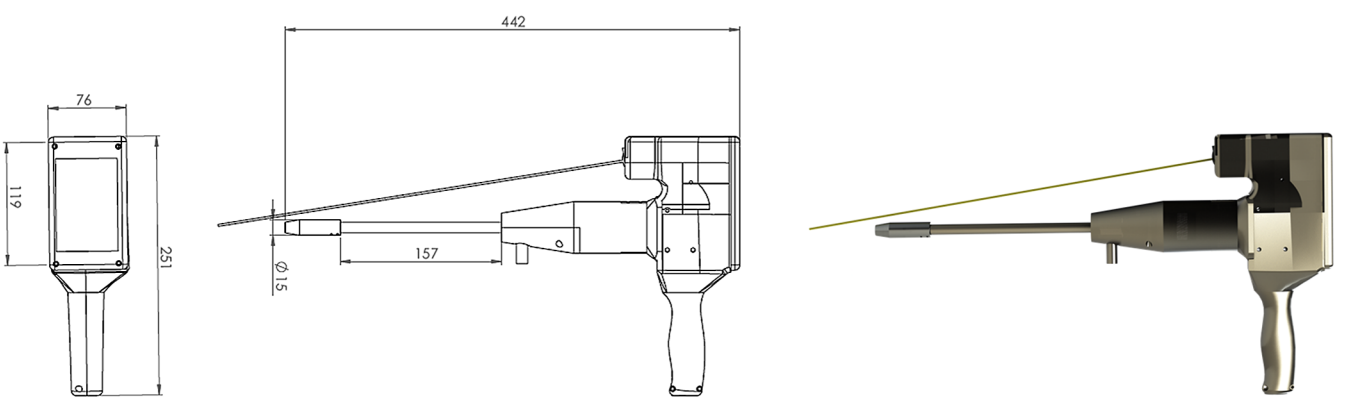

Fig. 15 Technical drawing of the scanner head for the presentation of relevant geometric features (Appendix).

subjects included in this pilot study are developers of the applied OCT system and main author of the paper who decided to be volunteers on their own responsibility. Accordingly, the responsible local ethics committee waived the need for an approval. The study followed the tenets of the Declaration of Helsinki and was conducted in compliance with Health Insurance Portability and Accountability Act. Furthermore, the authors declare that there are no conflicts of interest related to this article.

Acknowledgments

For the presented research, we would like to thank Karl Storz GmbH & Co. KG, Tuttlingen, Germany, for provision of the rigid NIR endoscope. The author Florian Tetschke is supported by the European Union/European Social Fund (ESF) and the Free State of Saxony within the ESF junior research group "Optical Technologies in Medicine" (project number 100270108). The author Jonas Golde is supported by the European Union/European Social Fund (ESF) and the Free State of Saxony within a doctoral scholarship (project number 100284305).

References

1. D. Huang et al., "Optical coherence tomography," *Science* **254**, 1178–1181 (1991).
2. A. F. Fercher et al., "Optical coherence tomography-principles and applications," *Rep. Prog. Phys.* **66**(2), 239–303 (2003).
3. J. Walther et al., "Optical coherence tomography in biomedical research," *Anal. Bioanal. Chem.* **400**(9), 2721–2743 (2011).
4. S. Marschall et al., "Optical coherence tomography-current technology and applications in clinical and biomedical research," *Anal. Bioanal. Chem.* **400**(9), 2699–2720 (2011).
5. P. Wilder-Smith et al., "In vivo optical coherence tomography for the diagnosis of oral malignancy," *Lasers Surg. Med.* **35**(4), 269–275 (2004).
6. W. Jung et al., "Advances in oral cancer detection using optical coherence tomography," *IEEE J. Sel. Top. Quantum Electron.* **11**(4), 811–817 (2005).
7. P. Pande et al., "Automated classification of optical coherence tomography images for the diagnosis of oral malignancy in the hamster cheek pouch," *J. Biomed. Opt.* **19**(8), 086022 (2014).
8. C. K. Lee et al., "Diagnosis of oral submucous fibrosis with optical coherence tomography," *J. Biomed. Opt.* **14**(5), 054008 (2009).
9. S. Prestin et al., "Measurement of epithelial thickness within the oral cavity using optical coherence tomography," *Head Neck* **34**(12), 1777–1781 (2012).
10. I. Grulkowski et al., "Quantitative assessment of oral mucosa and labial minor salivary glands in patients with Sjögren's syndrome using swept source OCT," *Biomed. Opt. Express* **5**(1), 259–274 (2014).
11. R. A. Leitgeb et al., "Doppler optical coherence tomography," *Prog. Retinal Eye Res.* **41**(100), 26–43 (2014).
12. J. Walther et al., "Analysis of in vitro and in vivo bidirectional flow velocities by phase-resolved Doppler Fourier-domain OCT," *Sens. Actuators A: Phys.* **156**(1), 14–21 (2009).
13. J. Walther and E. Koch, "Relation of joint spectral and time domain optical coherence tomography (jSTdOCT) and phase-resolved Doppler OCT," *Opt. Express* **22**(19), 23129–23146 (2014).
14. J. F. de Boer, C. K. Hitzenberger, and Y. Yasuno, "Polarization sensitive optical coherence tomography–a review," *Biomed. Opt. Express* **8**(3), 1838–1873 (2017).
15. B. Baumann, "Polarization sensitive optical coherence tomography: a review of technology and applications," *Appl. Sci.* **7**(5), 474 (2017).
16. M. Pircher, C. K. Hitzenberger, and U. Schmidt-Erfurth, "Polarization sensitive optical coherence tomography in the human eye," *Prog. Retinal Eye Res.* **30**(6), 431–451 (2011).
17. U. Morgner et al., "Spectroscopic optical coherence tomography," *Opt. Lett.* **25**(2), 111–113 (2000).
18. D. J. Faber et al., "Toward assessments of blood oxygen saturation by spectroscopic optical coherence tomography," *Opt. Lett.* **30**(9), 1015–1017 (2005).
19. Y. Shimada et al., "Noninvasive cross-sectional imaging of proximal caries using swept-source optical coherence tomography (SS-OCT) in vivo," *J. Biophotonics* **7**(7), 506–513 (2014).
20. P. Lenton et al., "Imaging in vivo secondary caries and ex vivo dental biofilms using cross-polarization optical coherence tomography," *Dent. Mater.* **28**(7), 792–800 (2012).
21. T. Louie et al., "Clinical assessment of early tooth demineralization using polarization sensitive optical coherence tomography," *Lasers Surg. Med.* **42**(10), 898–905 (2010).
22. L. L. Otis et al., "Optical coherence tomography: a new imaging technology for dentistry," *J. Am. Dent. Assoc.* **131**(4), 511–514 (2000).
23. C. Wilder-Smith et al., "Quantification of dental erosions in patients with GERD using optical coherence tomography before and after double-blind, randomized treatment with esomeprazole or placebo," *Am. J. Gastroenterol.* **104**(11), 2788–2795 (2009).
24. H. Nakagawa et al., "Validation of swept source optical coherence tomography (SS-OCT) for the diagnosis of smooth surface caries in vitro," *J. Dent.* **41**(1), 80–89 (2013).
25. J. A. Warren et al., "Imaging and characterization of dental structure using optical coherence tomography," in *Technical Digest. Summaries of papers presented at the Conf. on Lasers and Electro-Optics (CLEO '98)*, Vol. 6, p. 128 (1998).
26. S. K. Manesh, C. L. Darling, and D. Fried, "Imaging natural and artificial demineralization on dentin surfaces with polarization sensitive optical coherence tomography," *Proc. SPIE* **6843**, 68430M (2008).
27. S. K. Manesh, C. L. Darling, and D. Fried, "Polarization-sensitive optical coherence tomography for the nondestructive assessment of the remineralization of dentin," *J. Biomed. Opt.* **14**(4), 044002 (2009).
28. P. Wilder-Smith et al., "Optical diagnostics in the oral cavity: an overview," *Oral Dis.* **16**(8), 717–728 (2010).
29. Y. S. Hsieh et al., "Dental optical coherence tomography," *Sensors* **13**(7), 8928–8949 (2013).
30. S. Canjau et al., "Optical coherence tomography for non-invasive ex vivo investigations in dental medicine–a joint group experience," *Mod. Technol. Med.* **7**(1), 97–114 (2015).
31. Y. Shimada et al., "Application of optical coherence tomography (OCT) for diagnosis of caries, cracks, and defects of restorations," *Curr. Oral Health Rep.* **2**(2), 73–80 (2015).
32. D. Fried et al., "Imaging caries lesions and lesion progression with polarization sensitive optical coherence tomography," *J. Biomed. Opt.* **7**(4), 618–627 (2002).
33. M. H. Van der Veen, "Detecting short-term changes in the activity of caries lesions with the aid of new technologies," *Curr. Oral Health Rep.* **2**(2), 102–109 (2015).
34. D. Ericson et al., "Minimally invasive dentistry–concept and techniques in cariology," *Oral Health Prev. Dent.* **1**(1), 59–72 (2003).
35. M.-T. Tsai et al., "Effective indicators for diagnosis of oral cancer using optical coherence tomography," *Opt. Express* **16**(20), 15847–15862 (2008).
36. M.-T. Tsai et al., "Differentiating oral lesions in different carcinogenesis stages with optical coherence tomography," *J. Biomed. Opt.* **14**(4), 044028 (2009).
37. C.-K. Lee et al., "Diagnosis of oral precancer with optical coherence tomography," *Biomed. Opt. Express* **3**(7), 1632–1646 (2012).
38. Z. Hamdoon et al., "Structural validation of oral mucosal tissue using optical coherence tomography," *Head Neck Oncol.* **4**(1), 29 (2012).
39. Z. Hamdoon et al., "Optical coherence tomography in the assessment of suspicious oral lesions: an immediate ex vivo study," *Photodiagn. Photodyn. Ther.* **10**(1), 17–27 (2013).
40. Z. Hamdoon et al., "Optical coherence tomography in the assessment of oral squamous cell carcinoma resection margins," *Photodiagn. Photodyn. Ther.* **13**, 211-217 (2016).
41. B. A. Miles, "How close are we to real time optical margin control in head and neck oncologic surgery?" *Cancer Cell Microenviron.* **3**(2), 1305 (2016).
42. G. Tirelli et al., "Will the mininvasive approach challenge the old paradigms in oral cancer surgery?" *Eur. Arch. Oto-Rhino-Laryngol.* **274**(3), 1279–1289 (2017).
43. M. J. Gora et al., "Endoscopic optical coherence tomography: technologies and clinical applications," *Biomed. Opt. Express* **8**(5), 2405–2444 (2017).
44. G. G. J. Tearney et al., "Scanning single-mode fiber optic catheter-endoscope for optical coherence tomography," *Opt. Lett.* **21**(7), 543–545 (1996).
45. G. J. Tearney et al., "In vivo endoscopic optical biopsy with optical coherence tomography," *Science* **276**(5321), 2037–2039 (1997).
46. G. J. Tearney et al., "Consensus standards for acquisition, measurement, and reporting of intravascular optical coherence tomography studies: a report from the International Working Group for intravascular optical

coherence tomography standardization and validation," *J. Am. Coll. Cardiol.* **59**(12), 1058–1072 (2012).
47. N. Hanna et al., "Two-dimensional and 3-dimensional optical coherence tomographic imaging of the airway, lung, and pleura," *J. Thorac. Cardiovasc. Surg.* **129**(3), 615–622 (2005).
48. T. H. Tsai et al., "Ultrahigh speed endoscopic optical coherence tomography for gastroenterology," *Biomed. Opt. Express* **5**(12), 4387–4404 (2014).
49. T. S. Kirtane and M. S. Wagh, "Endoscopic optical coherence tomography (OCT): advances in gastrointestinal imaging," *Gastroenterol. Res. Pract.* **2014**, 376367 (2014).
50. A. Burkhardt et al., "Endoscopic optical coherence tomography device for forward imaging with broad field of view," *J. Biomed. Opt.* **17**(7), 071302 (2012).
51. Z. Hubler et al., "Real-time automated thickness measurement of the in vivo human tympanic membrane using optical coherence tomography," *Quant. Imaging Med. Surg.* **5**(1), 69–77 (2015).
52. N. H. Cho et al., "Optical coherence tomography for the diagnosis and evaluation of human otitis media," *J. Korean Med. Sci.* **30**(3), 328–335 (2015).
53. L. Scolaro et al., "High-sensitivity anastigmatic imaging needle for optical coherence tomography," *Opt. Lett.* **37**(24), 5247–5249 (2012).
54. K. M. Kennedy et al., "Needle optical coherence elastography for the measurement of microscale mechanical contrast deep within human breast tissues," *J. Biomed. Opt.* **18**(12), 121510 (2013).
55. B. G. Muller et al., "Prostate cancer diagnosis: the feasibility of needle-based optical coherence tomography," *J. Med. Imaging* **2**(3), 037501 (2015).
56. M. Villiger et al., "Deep tissue volume imaging of birefringence through fibre-optic needle probes for the delineation of breast tumour," *Sci. Rep.* **6**, 28771 (2016).
57. F. I. Feldchtein et al., "In vivo OCT imaging of hard and soft tissue of the oral cavity," *Opt. Express* **3**(3), 239–251 (1998).
58. R. Brandenburg, B. Haller, and C. Hauger, "Real-time in vivo imaging of dental tissue by means of optical coherence tomography (OCT)," *Opt. Commun.* **227**(4–6), 203–211 (2003).
59. B. Davoudi et al., "Noninvasive in vivo structural and vascular imaging of human oral tissues with spectral domain optical coherence tomography," *Biomed. Opt. Express* **3**(5), 826–839 (2012).
60. M.-T. Tsai et al., "Noninvasive structural and microvascular anatomy of oral mucosae using handheld optical coherence tomography," *Biomed. Opt. Express* **8**(11), 5001–5012 (2017).
61. J. M. Ridgeway et al., "In vivo optical coherence tomography of the human oral cavity and oropharynx," *Arch. Otolaryngol. Head Neck Surg.* **132**(10), 1074–1081 (2006).
62. L. M. Higgins and M. C. Pierce, "Design and characterization of a hand-held multimodal imaging device for the assessment of oral epithelial lesions," *J. Biomed. Opt.* **19**(8), 086004 (2014).
63. J. Wang et al., "Development of a hybrid Raman spectroscopy and optical coherence tomography technique for real-time in vivo tissue measurements," *Opt. Lett.* **41**(13), 3045–3048 (2016).
64. D. Wang et al., "Endoscopic swept-source optical coherence tomography based on a two-axis microelectromechanical system mirror," *J. Biomed. Opt.* **18**(8), 086005 (2013).
65. C.-W. Sun, Y. Ho, and S. Lee, "Sensing of tooth microleakage based on dental optical coherence tomography," *J. Sens.* **2014**, 984627 (2014).
66. A. M. D. Lee et al., "Wide-field in vivo oral OCT imaging," *Biomed. Opt. Express* **6**(7), 2664–2674 (2015).
67. H. Shemesh et al., "The ability of optical coherence tomography to characterize the root canal walls," *J. Endod.* **33**(11), 1369–1373 (2007).
68. M. Wojtkowski et al., "Ultrahigh-resolution, high-speed, Fourier domain optical coherence tomography and methods for dispersion compensation," *Opt. Express* **12**(11), 2404–2422 (2004).
69. F. Köttig et al., "An advanced algorithm for dispersion encoded full range frequency domain optical coherence tomography," *Opt. Express* **20**(22), 24925–24948 (2012).
70. J. Walther et al., "Signal power decrease due to fringe washout as an extension of the limited Doppler flow measurement range in spectral domain optical coherence tomography," *J. Biomed. Opt.* **15**(4), 041511 (2010).
71. B. Cense et al., "Ultrahigh-resolution high-speed retinal imaging using spectral-domain optical coherence tomography," *Opt. Express* **12**(11), 2435–2447 (2004).
72. L. Pan et al., "Depth-dependent dispersion compensation for full-depth OCT image," *Opt. Express* **25**(9), 10345–10354 (2017).
73. C. Schnabel, M. Gaertner, and E. Koch, "Optical coherence tomography (OCT) for time-resolved imaging of alveolar dynamics in mechanically ventilated rats," *Appl. Sci.* **7**(3), 287 (2017).
74. K. J. Park, H. Schneider, and R. Haak, "Assessment of interfacial defects at composite restorations by swept source optical coherence tomography," *J. Biomed. Opt.* **18**(7), 076018 (2013).
75. K. Ishibashi et al., "Swept-source optical coherence tomography as a new tool to evaluate defects of resin-based composite restorations," *J. Dent.* **39**(8), 543–548 (2011).
76. Y. Chen et al., "Characterization of dentin, enamel, and carious lesions by a polarization-sensitive optical coherence tomography system," *Appl. Opt.* **44**(11), 2041–2048 (2005).
77. Y. Chen, L. Otis, and Q. Zhu, "Polarization memory effect in optical coherence tomography and dental imaging application," *J. Biomed. Opt.* **16**(8), 086005 (2011).
78. P. Cimalla et al., "Simultaneous dual-band optical coherence tomography in the spectral domain for high resolution in vivo imaging," *Opt. Express* **17**(22), 19486–19500 (2009).
79. J.-M. Kim, S.-R. Kang, and W.-J. Yi, "Automatic detection of tooth cracks in optical coherence tomography images," *J. Periodontal Implant Sci.* **47**(1), 41–50 (2017).
80. K. Imai et al., "Noninvasive cross-sectional visualization of enamel cracks by optical coherence tomography in vitro," *J. Endod.* **38**(9), 1269–1274 (2012).
81. H. Kakuma, K. Ohbayashi, and Y. Arakawa, "Optical imaging of hard and soft dental tissues using discretely swept optical frequency domain reflectometry optical coherence tomography at wavelengths from 1560 to 1600 nm," *J. Biomed. Opt.* **13**(1), 014012 (2008).
82. K. J. Park, H. Schneider, and R. Haak, "Assessment of defects at tooth/self-adhering flowable composite interface using swept-source optical coherence tomography (SS-OCT)," *Dent. Mater.* **31**(5), 534–541 (2015).
83. K. Horie et al., "Monitoring of cariogenic demineralization at the enamel-composite interface using swept-source optical coherence tomography," *Dent. Mater.* **32**(9), 1103–1112 (2016).

Julia Walther is a senior researcher at Technische Universität Dresden. She received her diploma degree in physics technology and biomedical engineering from the University of Applied Sciences Mittweida in 2006 and her PhD degree in medical physics and biomedical optics from the Technische Universität (TU) Dresden in 2010. Her current research interests include the advancement of optical coherence tomography for different applications in dentistry and otolaryngology as well as the analysis and extension of diverse theoretical models for Doppler OCT (DOCT).

Christian Schnabel finished his studies of physical engineering at the University of Applied Sciences Mittweida in 2010 and subsequently joined the Department of Clinical Sensoring and Monitoring at the Faculty of Medicine Carl Gustav Carus in Dresden. He received his PhD degree in 2015 in the field of lung imaging, mechanical ventilation, and total liquid ventilation. His main field of research is currently the imaging of different biological tissues by optical coherence tomography.

Florian Tetschke received his MSc degree in biomedical engineering from the University of Applied Sciences, Jena, in 2013. He contributed to research projects at the Biomagnetic Center of the University Hospital in Jena, at the Polytechnical University of Catalonia and the Institute of Biomedical Engineering at the Technische Universität Dresden. Currently, he is a research associate at the young scientist group, "Optical Technologies in Medicine" at Technische Universität Dresden. His research interest focuses on the development and application of optical technologies, such as hyperspectral imaging, optical coherence tomography, and Raman spectroscopy.

Tobias Rosenauer is a dentist and a research associate of the University Clinic Carl Gustav Carus in Dresden. He graduated in 2016 and has since then worked for the Department of Operative Dentistry, TU Dresden. He is currently writing his doctoral thesis and his present research concerns cariological aspects as well as optical imaging.

Jonas Golde is a PhD student at the Technische Universität Dresden. He received his MSc degree in physics from the Technische Universität Dresden in 2016 with a thesis on polarization sensitive optical coherence tomography (PS-OCT). Since then, he has been focused on the development and application of PS-OCT systems in the fields of dentistry and otolaryngology. His research interests include the combination of PS-OCT with complementary optical technologies, such as multiphoton microscopy and hyperspectral imaging.

Christian Hannig is the head of the department of Operative Dentistry, TU Dresden. Furthermore, he is the dean for dental education. He is a dentist since 2000 and has worked at Göttingen and Freiburg University before coming to Dresden. His main field of research is bioadhesion in the oral cavity. He is the author of more than 100 international and national journal papers. His research has been funded several times by the German Research Foundation.

Edmund Koch received his diploma and PhD degrees in physics from the University of Marburg. He worked as a senior researcher at the Drägerwerke AG, Lübeck, and thereafter, he became professor for laser and optics at the Lübeck University of Applied Sciences. He is currently head of the work group Clinical Sensoring and Monitoring at the Faculty of Medicine at the TU Dresden. His main research interests are optical coherence tomography and spectroscopic imaging.

Biographies for the other authors are not available.